Testing of a novel bio-inspired passive actuator for structural control

I Y Kwon[1], H T Yang[1], P K Hansma[2], and C J Randall[1]

[1] Department of Mechanical Engineering, University of California, Santa Barbara, CA 93106, USA
[2] Department of Physics, University of California, Santa Barbara, CA 93106, USA

Abstract. A bio-inspired passive actuator inspired by an energy dissipating mechanism called 'sacrificial bonds and hidden length' is designed, fabricated and implemented in a test case of a three-story structural model for testing its performance and effectiveness for passive controlling structural responses. A new type of element in the current dynamic system called a 'negative spring' is used to optimize passive damping based on a recently developed method: Force, Distance and Velocity (FDV) plots optimized with a Linear Quadratic Regulator LQR feedback controller. This novel actuator can give a relatively higher force output at a much more affordable cost, which makes the bio-inspired passive actuator more practical for implementation in real structures. Numerical prediction with experimental validation for the illustrative examples suggests that the bio-inspired passive actuator with currently designed negative spring has comparable performance to state-of-the-art semi-active actuators. It could thus be developed to become a practical, low cost, electrically free, and effective passive control device for practical use in actual civil, mechanical, aerospace, and other structures.

1. Introduction

The amazing fracture resistant performance of abalone shell (Evans *et al.* 2001, Schaffer *et al.* 1997, Fritz *et al.* 1994, Zaremba *et al.* 1996) and bone (Thompson *et al*. 2001, Hansma *et al*. 2005, Fantner *et al*. 2006b, 2007) has been studied by various researchers. Abalone shells and bones contain sacrificial bonds and hidden length (Smith *et al*. 1999, Fantner *et al*. 2005, 2006a) that stretch after initial break under load, then reform back to its original form when unloaded. The energy required to stretch the bond is two orders of magnitude higher than the energy required to break the initial bond. This mechanism has inspired the development of a new concept of energy dissipating passive actuator for control of civil infrastructures in resistance of disturbances such as earthquakes or winds (Yang *et al*. 2010), and of aeronautical vehicles in resistance of aerodynamic forces that could cause flutter.

As an effort to develop a highly efficient passive actuator, a concept of bio-inspired passive actuator was presented by the present research group (Yang *et al*. 2010). A numerical model of a bio-inspired passive actuator was designed as a combination of negative spring, damper and the mechanical behavior of sacrificial bond-hidden length of abalone shell. The performance of the bio-inspired passive actuator, estimated through

numerical simulation, was comparable to the state-of-the-art active and semi-active actuators (Dyke *et al*. 1996b, Scruggs and Iwan 2003). An experimental model of a passive actuator exhibiting the behavior of negative spring using permanent magnets was introduced, built, and tested. Due to the usage of permanent magnets, the experimental model presented difficulty of achieving large enough force output for controlling civil structures. While the concept of bio-inspired passive actuator presented great performance potential in structural control, achieving the desired magnitude of force in large scale experiment remains a challenge and it has become the subject of this research and development.

The focus of this study is to create and test a new type of negative spring passive actuator, experimentally demonstrate its capability, and validate its accuracy by comparing the experimental results with numerical predictions. Improvements are made by removing the use of magnets from the design and also implementing adjustable maximum force capacity. The new design allows the actuator to be easily scaled and implemented into a variety of realistic structures such as tall buildings, bridges, aircraft wings, etc.

In addition to the experimental validation of the numerical model, the actuator's performance in structural response reduction is also evaluated. Specifically in the evaluation, the ability of the system to reduce the peak responses in the case of the earthquake excitation is studied.

This study includes a specific novel design of the new negative spring combined with dashpot damper which exhibits the mechanism of the negative sacrificial bond-hidden length. This focus is approached in three steps. First, a newly constructed three-story model structure is introduced. The design and optimization of the new bio-inspired passive actuator with negative spring are then discussed. Lastly, the experimental results including the system setup description, demonstration, evaluation and validation are discussed.

2. Identification of the three-story model structure

Figure 1 is a diagram of the passively controlled, three-story model newly constructed specifically for the current study. The test structure is subjected to a one-dimensional ground motion, and it has diagonal trusses to restrict motion to the same direction. The building frame and the floors are constructed using aluminum, with a height of 165 cm. Each of the three floor masses of the model structure weighs 11.1 kg.

Efforts were made to obtain a mathematically accurate model for the test model structure in order to construct numerical simulation. Efforts were made to limit the amplitudes of vibrations of the shaking model so that the response of the structure is assumed to be within geometrically linear range. In practice, excitations and the structural response are maintained under 2 percent of the height of the structure so the assumption of geometric linearity is valid.

The equation of motion (Craig Jr 1981) of the model structure can be written as

$$\mathbf{M}_s\ddot{x} + \mathbf{C}_s\dot{x} + \mathbf{K}_s x = \Gamma f - \mathbf{M}_s\Lambda\ddot{x}_g \tag{1}$$

where x is a vector of the displacements of each floor, $\ddot{x}_g$ is a one-dimensional ground acceleration, f is the control force applied by the actuator installed on the structure. The mass, damping, stiffness matrices and the forcing and acceleration vectors, respectively, are defined as follows

$$\mathbf{M}_s = \begin{bmatrix} 10.8 & 0 & 0 \\ 0 & 10.83 & 0 \\ 0 & 0 & 10.83 \end{bmatrix} \text{kg} \tag{2}$$

$$\mathbf{C}_s = \begin{bmatrix} 4.88 & -1.40 & -0.30 \\ -1.40 & 4.52 & -1.71 \\ -0.30 & -1.71 & 3.08 \end{bmatrix} \frac{\mathrm{N \cdot s}}{\mathrm{m}}$$

$$\mathbf{K}_s = 10^3 \begin{bmatrix} 12.1 & -5.97 & 0.03 \\ -5.97 & 11.9 & -5.94 \\ 0.03 & -5.94 & 5.91 \end{bmatrix} \frac{\mathrm{N}}{\mathrm{m}}$$

$$\Gamma = \begin{bmatrix} 1 \\ 0 \\ 0 \end{bmatrix} \qquad \Lambda = \begin{bmatrix} 1 \\ 1 \\ 1 \end{bmatrix}$$

Equation (1) can be rewritten in state-space form as

$$\dot{z} = \mathbf{A}z + \mathbf{B}f + \mathbf{E}\ddot{x}_g \tag{2}$$

where z is the state vector. The measurement equation is given by

$$y = \mathbf{C}z + \mathbf{D}f + v \tag{3}$$

where y is the vector of measured outputs, v is the noise vector in measurement. The structural measurements required to construct the FDV plot are the displacement and the velocity of each floor (i.e., $y = [x_1 \quad x_2 \quad x_3 \quad \dot{x}_1 \quad \dot{x}_2 \quad \dot{x}_3]'$). The acceleration measurements of each floor are also required to evaluate the performance of the actuator (i.e., $y = [\ddot{x}_{a1} \quad \ddot{x}_{a2} \quad \ddot{x}_{a3}]'$). Thus, the state-space matrices **A**, **B**, **C**, **D** and **E** are defined as

$$\mathbf{A} = \begin{bmatrix} \mathbf{0} & \mathbf{I} \\ -\mathbf{M_s}^{-1}\mathbf{K_s} & -\mathbf{M_s}^{-1}\mathbf{C_s} \end{bmatrix} \quad \mathbf{B} = \begin{bmatrix} \mathbf{0} \\ \mathbf{M_s}^{-1}\mathbf{\Gamma} \end{bmatrix} \quad \mathbf{E} = -\begin{bmatrix} \mathbf{0} \\ \mathbf{\Lambda} \end{bmatrix} \tag{4}$$

and

$$\mathbf{C} = \begin{bmatrix} -\mathbf{M_s}^{-1}\mathbf{K_s} & -\mathbf{M_s}^{-1}\mathbf{C_s} \\ \mathbf{I} \end{bmatrix} \quad \mathbf{D} = \begin{bmatrix} \mathbf{M_s}^{-1}\mathbf{\Gamma} \\ \mathbf{0} \end{bmatrix} \tag{5}$$

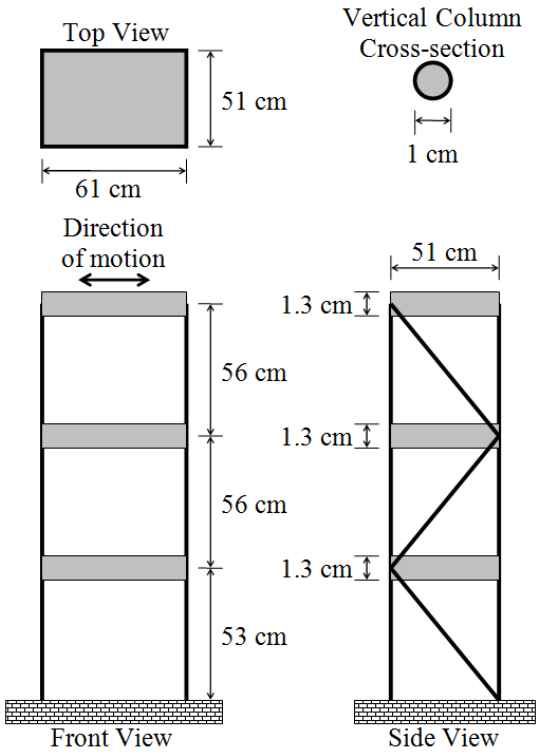

Figure 1. Three-story aluminum test model structure.

3. Optimal passive actuator

In an effort to find an optimized control for the bio-inspired passive actuator, a simple optimization method utilizing a contour plot of force versus displacement and velocity (FDV) based on linear quadratic regulator control is generated, as proposed previously (Yang *et al*. 2010). The method consists of two steps: (i) finding an optimal controller of the structural response for a specifically selected earthquake, (ii) designing a passive actuator by mimicking the FDV plot of the optimal controller. Actuators with similar FDV diagram may be expected to have similar performance. Designing a passive actuator by replicating the FDV plot of an optimal controller may be a worthy novel way to construct an optimal passive actuator.

An optimal controller was obtained with linear quadratic regulator (LQR) optimization (Kwakernaak and Sivan, 1972). For a continuous time system, the state-feedback law $f = -\mathbf{K}x$ minimizes the quadratic cost function of

$$J = \lim_{t\to\infty}\int_0^t \left(y^T \mathbf{Q} y + f^T \mathbf{R} f \right) dt \tag{6}$$

where $\mathbf{Q}$ and $\mathbf{R}$ are symmetric positive-definite matrices that defines the criterion of the control performance. There exist infinitely many LQR controllers for a single system. In structural control, different $\mathbf{Q}$ and $\mathbf{R}$ should be used to accomplish different structural response reduction performance criteria for the target model structure. $\mathbf{K}$ is the full state feedback gain matrix for the deterministic regular problem given by

$$\mathbf{K} = \mathbf{R}^{-1}\left(\mathbf{B}^T \mathbf{P}\right) \tag{7}$$

where $\mathbf{P}$ is the solution to the associated algebraic Riccati equation given by

$$\mathbf{A}^T\mathbf{P} + \mathbf{P}\mathbf{A} - (\mathbf{P}\mathbf{B})\mathbf{R}^{-1}(\mathbf{B}^T\mathbf{P}) + \mathbf{C}^T\mathbf{Q}\mathbf{C} = 0. \tag{8}$$

The calculation to determine $\mathbf{K}$ is performed using the control toolbox in MATLAB.

In this simulation, the three-story test structure is excited with the ground acceleration of the north-south component of 1940 El Centro earthquake shown in figure 2. Since the test structure is a scaled model, the earthquake is simulated at a rate five times faster (Dyke *et al*., 1996b). In addition, the amplitude of the earthquake acceleration is reduced to 60 percent of its original value to keep the structural response within geometrically linear region. A wide variety of controllers are evaluated while focusing on minimizing the first floor displacement and the third floor acceleration. After careful comparison of the peak structural response results, the LQR controller with minimum first floor displacement and third floor acceleration were obtained using $\mathbf{R} = 0.2$, $\mathbf{Q}_{33} = 746$ and $\mathbf{Q}_{44} = 3787$. All the other elements of Q are zero. The resulting cost function can be written as.

$$J = \lim_{t\to\infty}\int_0^t \left(1.79\times10^3 \ddot{x}_3^2 + 5.19\times10^6 x_1^2 + 0.2 f_1^2\right)dt \tag{9}$$

The resulting optimal control force-displacement-velocity plot is shown in figure 3(a). Since the target model structure is different, the cost function and the FDV plot are different from those of the previous publication (Yang *et al*. 2010), as shown in figure 3(b). Although both of the cost functions of the LQR control are chosen to minimize the first floor displacement and third floor acceleration of each structure, there is a notable difference in overall profile of the FDV plot. However, both structures show the need for a combination of the negative spring and damping force to accomplish the optimal control. Discussions of the negative spring and the actuator design which mimics the optimal control will be given subsequently.

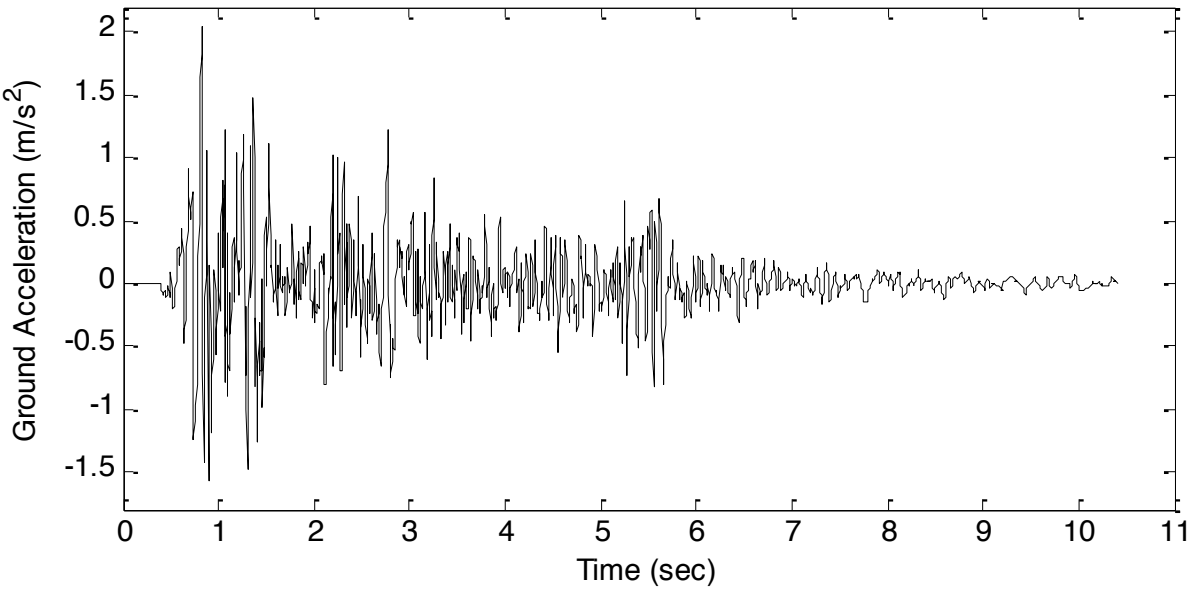

Figure 2. Reduced amplitude, time scaled NS component of 1940 El Centro earthquake.

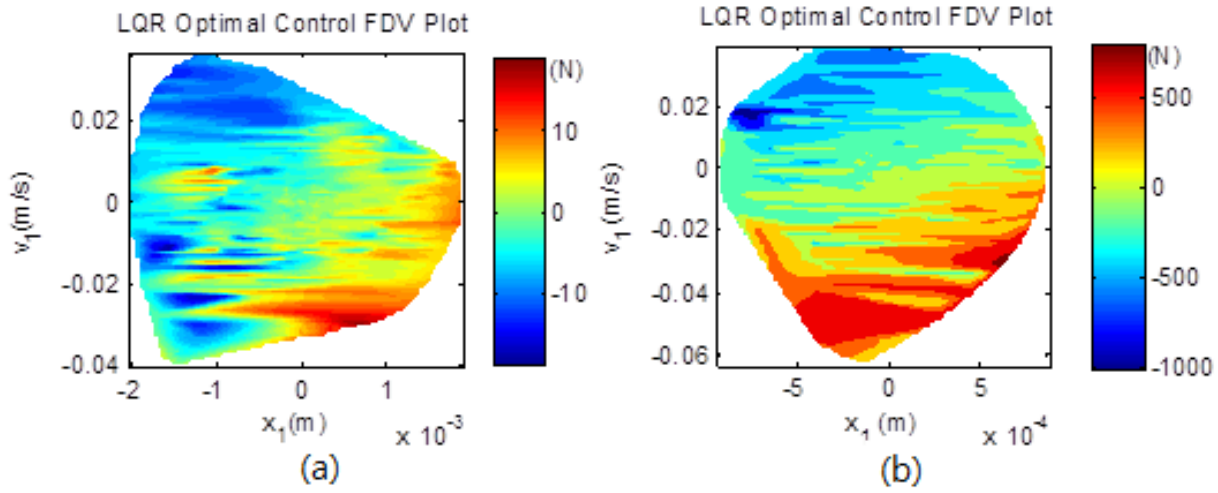

Figure 3. a) Force-Displacement-Velocity plots based on current three-story test structure over the north-south acceleration components of the scaled 1940 El Centro earthquake at a reduced amplitude with the LQR optimal control force based on the minimization of the cost function $J = \lim_{t\to\infty}\int_0^t \left(1.79\times10^3 \ddot{x}_3^2 + 5.19\times10^6 x_1^2 + 0.2 f_1^2\right)dt$; and b) FDV plot calculated by Yang (*et al*. 2010) based on the three-story model introduced by Dyke *et al* (1996) over the same earthquake at the original amplitude with LQR optimal control force based of the minimization of the cost function $J = \lim_{t\to\infty}\int_0^t \left(1.83\times10^6 \ddot{x}_3^2 + 7.2\times10^{12} x_1^2 + 1.0 f_1^2\right)dt$.

4. A new design of bio-inspired passive actuator

Force versus displacement and velocity (FDV) plots of optimized controllers for two different three-story test structures under the 1940 El Centro earthquake are shown in figure 3. Analyzing the FDV plots suggests a common requirement for optimal control. Both optimal controllers require a special forcing behavior such that, if a mass is moved out of equilibrium, it is pushed further away from the equilibrium. In fact, a combination of a dashpot damper and a negative spring is found to be able to form such FDV profile. A negative spring is a concept of a mechanical device which exerts force in the opposite direction as opposed to a conventional spring. For example, if a mass is out of equilibrium, the negative spring pushes the mass further away from the equilibrium. As the offset distance increases, the negative spring force also increases. Two different designs using the negative spring are discussed in the following subsections. The negative spring using magnets, previously introduced in Yang *et al* 2010, is discussed first. Then, a new design of negative spring, tailored to exhibit the behavior of negative sacrificial bond and hidden length more closely, is then discussed. However, both designs do not exhibit the completely linear force-displacement relationship conventionally implied by the mechanical spring. Figure 4 shows the force as the function of displacement presented by both devices. It is noted that the magnetic negative spring force rises to its maximum only at the displacement limits, while the mechanical negative spring force can have a defined maximum force throughout its displacement range.

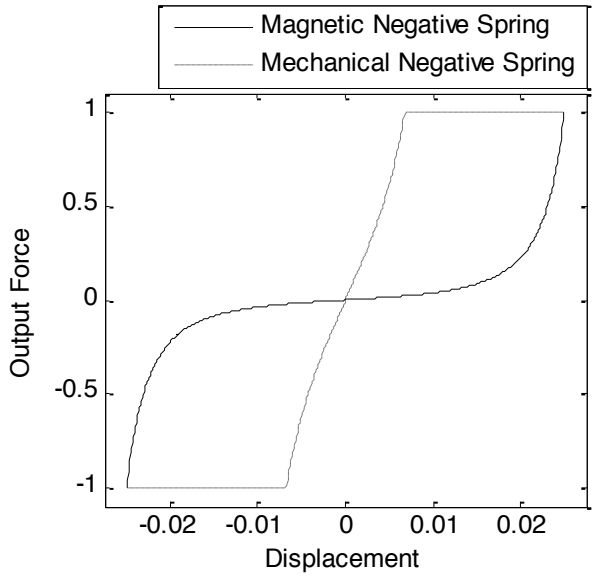

Figure 4. Force versus displacement plot of two negative spring devices.

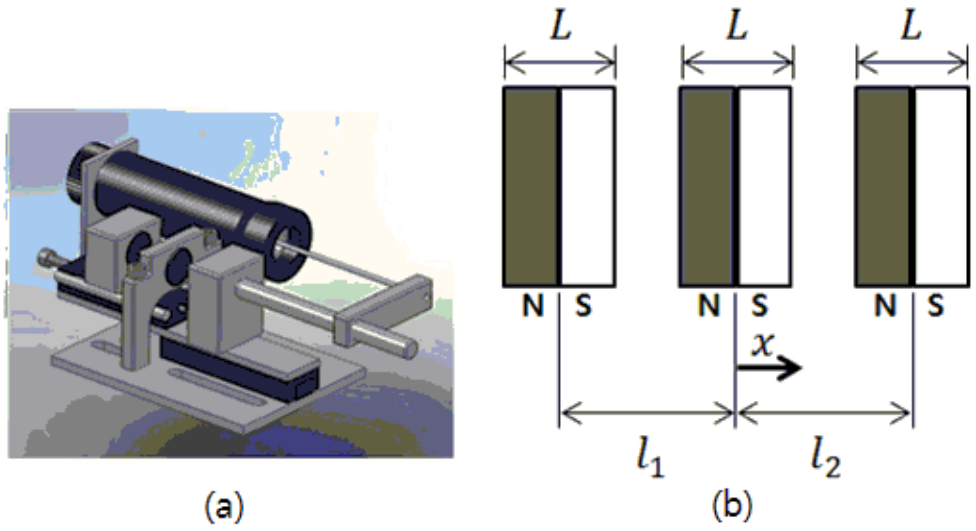

Figure 5. a) Negative spring with damping prototype device using magnets (Yang *et al*. 2010) and b) the alignment of three magnets showing the polarity.

4.1. Former design of negative spring actuator using permanent magnets

A design of negative spring using magnets is shown in figure 5(a). The negative spring with damping prototype device uses a commercial dashpot damper (the black cylinder) together with a novel element that uses three magnets. Two outer magnets on a linear slide are attracted to a stationary magnet that is held in the central component mounted on the base. The experimental result showed convincing agreement with the numerical simulation assuming linear force-displacement relationship for small displacement. The force-displacement relationship between magnets becomes nonlinear when displacement becomes relatively large. When three magnets are aligned to attract each other as shown in figure 5(b), the force as the function of the displacement of the center magnet, $f_{mag}(x)$, is expressed as,

$$f_{mag}(x) = \left[\frac{B_0^2 A^2 \left(L^2 + R^2\right)}{\pi \mu_0 L^2}\right]\left(f_2 - f_1\right)$$
$$f_1 = \frac{1}{|l_1 - x|^2} + \frac{1}{\left(|l_1 - x| + 2L\right)^2} + \frac{2}{\left(|l_1 - x| + L\right)^2} \quad (10)$$
$$f_2 = \frac{1}{|l_2 - x|^2} + \frac{1}{\left(|l_2 - x| + 2L\right)^2} + \frac{2}{\left(|l_2 - x| + L\right)^2}$$

where B_0 is the magnetic flux density very close to each pole, μ_0 is the permeability of space, which equals $4\pi \times 10^{-7}$ T·m/A, A is the area of each pole, L is the length of each magnet, R is the radius of each magnet, l_1 is the location of the magnet left to the center magnet, and l_2 is the location of the magnet right to the center magnet. The equation of the force between two magnets f_1 and f_2 are based on Gilbert's model (1600).

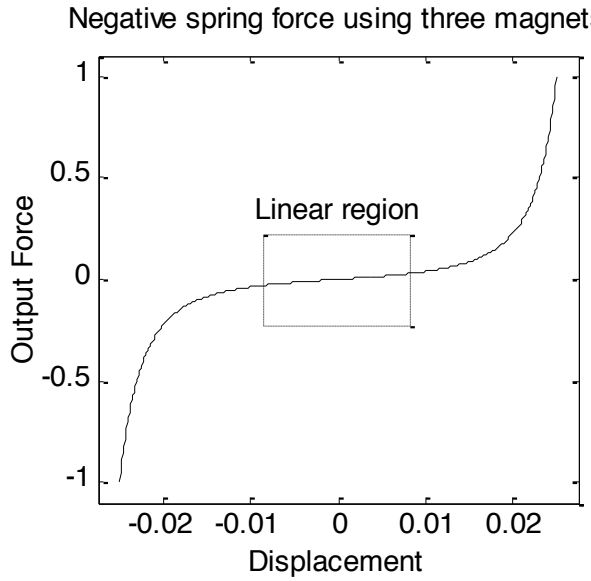

Figure 6. Plot of force versus displacement relationship of the negative spring designed with three magnets.

Figure 6 is a plot of the magnetic negative spring force behavior with its maximum force normalized to 1N. It is noted that the small linear region is the usable region for this design which has a much smaller magnitude in force, requiring very powerful magnets to reach appreciable force. The calculation of the force is based on equation 10. Although the force displacement curve is nonlinear, there is a small region around the equilibrium where the force curve appears to be relatively linear compared to the rest. It is observed that limiting the actuator to be operated in the linear region, as assumed in Yang (*et al* 2010), is utilizing only 3% of the full strength of the magnets. Such limitations make it challenging to design and fabricate actuator for practical use in full scale structures such as in buildings, bridges, airplane wings, and automobiles, etc. A more extensive case study assessing the feasibility of magnetic negative spring in an actual application is provided in section 7.

Actuator using permanent magnets may also present difficulty in handling during fabrication, transportation, installation, and operation. Permanent magnetic field passively attracts ferromagnetic objects when it is not desired to do so. Since high strength magnetic field may cause undesirable effects on electric devices. The

negative spring actuator with magnets operating while surrounded by electrically controlled apparatuses, such as that inside of a building or even an aircraft wing as an example with sensitive instruments, facilities, devices, may also be undesirable.

4.2. New design of bio-inspired passive actuator

Considering limitations of the magnetic based design of negative spring, it is desirable to search for alternative novel ideas. A simple idea using a conventional spring with a novel mechanical design is introduced. The design simply redirects the output force of the spring to the direction of building motion. Furthermore, the actuator can be easily scaled to produce high output forces for real structures as will be discussed in section 7. Using the negative spring force combined with dashpot damper properly, the actuator could actually exhibit the mechanism of the negative sacrificial bond and hidden length, thus resulting in a desired capability to control structure response reduction.

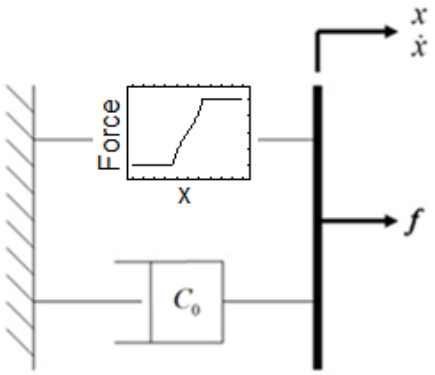

Figure 7. Simple mechanical model of the bio-inspired system.

A simple mechanical model of the new bio-inspired passive damper consisting of a damper and a negative spring is designed and shown in figure 7. The negative spring force output is shown in parallel with a conventional damper. A simple diagram of mechanical negative spring implementation is depicted in figure 8.

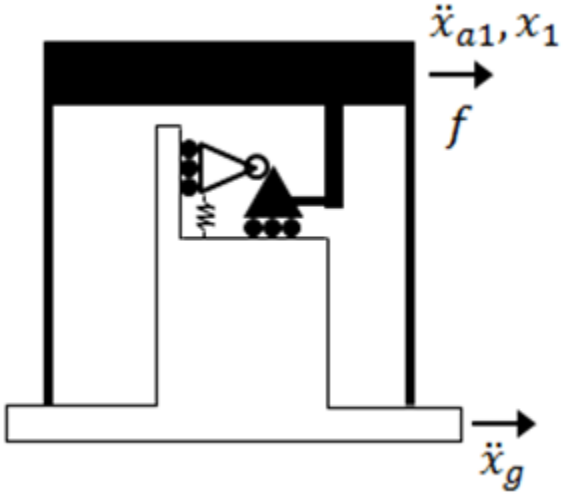

Figure 8. Diagram of mechanical negative spring actuator implementation.

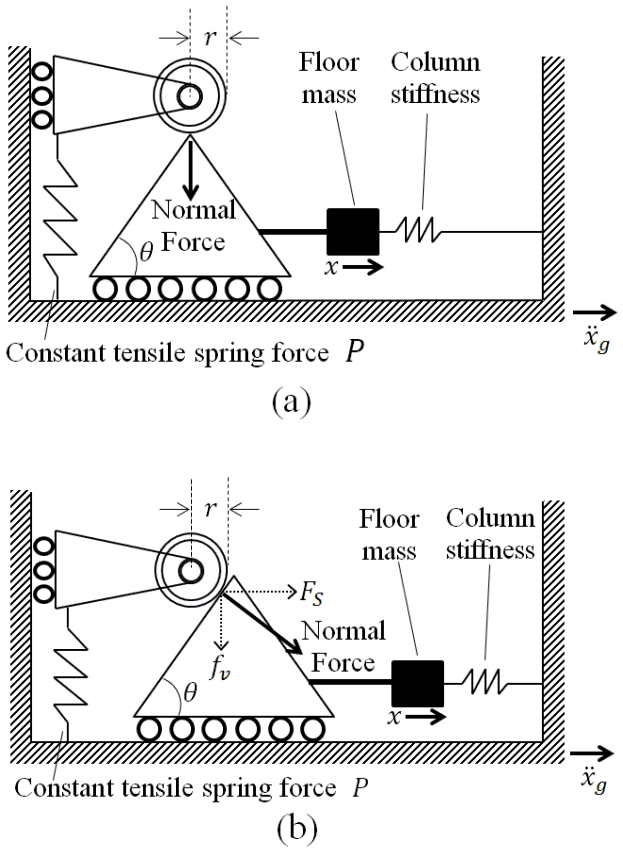

Figure 9. A simplified diagram of a negative spring actuator.

A simplified diagram of a negative spring actuator is shown in figure 9. A negative spring force is achieved through a special interaction between a roller, a triangle ramp, and a spring under constant tension. The pre-stretched spring can be assumed to have a constant spring tension for a small change of deflection. The mechanism of negative spring can be explained in the next paragraph.

The roller bearing is restricted to move only in vertical direction, and the ramp can only move horizontally. The two components are always in contact. A preloaded spring applies a constant down ward force, P, on a roller bearing. This results in a normal force at the contact surface between the roller and the ramp. The negative spring force is the horizontal component of the force exerted by the roller onto the ramp. At equilibrium, the actuator has no output force (case (a)) since the spring force is balanced by the normal force. The roller stays at the top of the ramp, exerting zero horizontal force on the ramp (figure 9(a)). When the structure is excited by an earthquake and moves from equilibrium by a distance, x, the roller would tip over, and the normal force will create a horizontal component, $F_S(x)$, as shown in (figure 9(b)). The horizontal force causes the ramp to be pushed further away from equilibrium, delivering the negative spring force to the structure. The roller may slide on each side of the ramp as the structure sways back and forth.

The negative spring force as a function of the structural displacement, denoted as $F_S(x)$, can be modeled mathematically.

$$F_S(x) = \begin{cases} P\tan\left(\sin^{-1}\left(\frac{|x|}{r}\right)\right) & if \quad r\sin(\theta) > x > 0 \\ -P\tan\left(\sin^{-1}\left(\frac{|x|}{r}\right)\right) & if \quad -r\sin(\theta) < x < 0 \\ P\tan(\theta)\frac{x}{|x|} & if \quad |x| \geq r\sin(\theta) \\ 0 & if \quad x = 0 \end{cases} \tag{11}$$

where P is the pre-stretched spring force, which is assumed to be constant, r is the radius of the roller bearing, and θ is the slope of the triangle ramp with respect to horizon. The slope θ is limited to $0^o < \theta < 90^o$. It is notable that the negative spring in this study does not have a linear force versus displacement relationship. As shown in figure 4, the control force quickly increases in a tangent function of the displacement, then plateaus with a constant force as described in equation 11.

Since the negative spring force naturally pushes structure away from its equilibrium, the maximum force limit which is set by the pre-stretched spring, provides a control to keep the negative force in a allowable boundary. The threshold displacement where the control force reaches its maximum is controlled by the radius of the roller and the slope. In other words, one can control not only how high the control force could be, but also how quickly it could reach its maximum capacity.

5. Experimental testing

5.1. Experimental setup

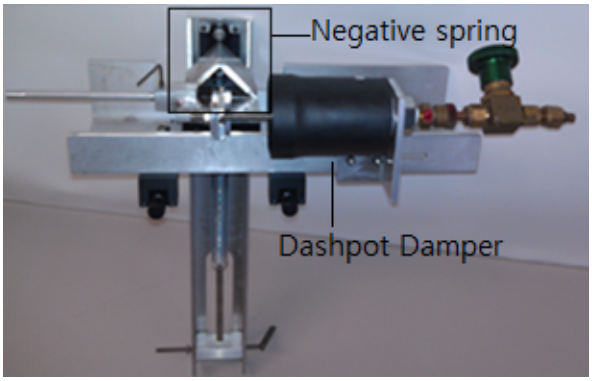

Figure 10. A bio-inspired passive actuator equipped with mechanical negative spring was built for conceptual design and experimental verification.

A bio-inspired passive actuator, displayed in figure 10, was built for conceptual design and experimental verification. The dashpot damper implemented in the actuator has a variable damping coefficient (0-2 $\mathrm{N}\cdot\mathrm{sec/cm}$), and it was manufactured by Airpot Corporation (2K444P). The negative spring is consists of a triangular ramp, a roller bearing, two sliders, a shaft, and a spring. The negative spring apparatus built for this study has a ± 2.5 cm stroke and fits within a volume of approximately $30\ \mathrm{cm} \times 30\ \mathrm{cm} \times 20\ \mathrm{cm}$. In practice, the ramp is fixed to the first floor, applying the control force to the first floor of the structure. The body of the actuator except the ramp is fixed to the ground. A simple diagram of actuator implementation is provided in

figure 8. The applied force f predicted by the model is

$$f = F_S(x) + C_0(\dot{x}) \tag{12}$$

where $F_S(x)$ is the force exerted by the negative spring apparatus (equation (11)), and C_0 is the damping coefficient. A series of carefully chosen parameters which are implemented to build the bio-inspired passive actuator are shown in table 1.

Table 1. Parameters of the bio-inspired passive actuator.

Parameter	Value
r	0.004763 m
P	16.5 N
θ	45°
C_0	90 N s/m

Two types of sensors are installed in the model structure for use in data analysis. Accelerometers are located on each floor to provide measurements of the absolute accelerations. Laser triangulation displacement sensors on each floor measure the displacement relative to the ground in order to evaluate the response reduction performance by the actuator. A force transducer is placed in series with the bio-inspired passive actuator to measure the control force being applied to the first floor of the structure. The reduced amplitude, and time scaled north-south component of the 1940 El Centro earthquake is used to excite the three-story test structure with the actuator installed between the ground and the first floor.

A linear electromagnetic positioning stage is implemented to shake the model structure with prescribed excitation. The stage has a travel range of 36 inches, and can provide up to 1,110 N continuous force and 3,330 N peak force. A 1 micron resolution non-contact linear encoder is incorporated into the stage to monitor stage position. LabVIEW software is used to drive the stage and also for data collection and sensor device management.

5.2. Experimental result

In the experiment, the structural response reduction ability of the model with bio-inspired passive actuator has been demonstrated and compared to the numerical simulation for validation. Figure 11 shows the comparison between the experimental measurement and the numerically simulated behavior of the bio-inspired passive actuator. The result in figure 11(a) shows a good agreement of control forces between the experimental measurement and the numerical prediction. The profile of the force-displacement-velocity (FDV) plots for both the experimental measurement (figure 11(b)) and the numerical simulation (figure 11(c)) also match quiet well, validating mutually the accuracy of the mathematical model, as well as the performance of the presently developed and fabricated actuator.

From the experiment, the bio-inspired passive actuator is able to reduce the peak third floor relative displacement by 63 percent and reduce the third floor absolute acceleration by 65 percent, as compared to the uncontrolled case.

The time response for the third floor displacement and the third floor absolute acceleration is shown in figure 12. It is noticed that the bio-inspired passive actuator was able to reduce the structural responses during the first few periods of motion. In addition, a comparison of the numerical prediction and the experimental measurement of the third floor response provide further validation of the accuracy of the mathematical model.

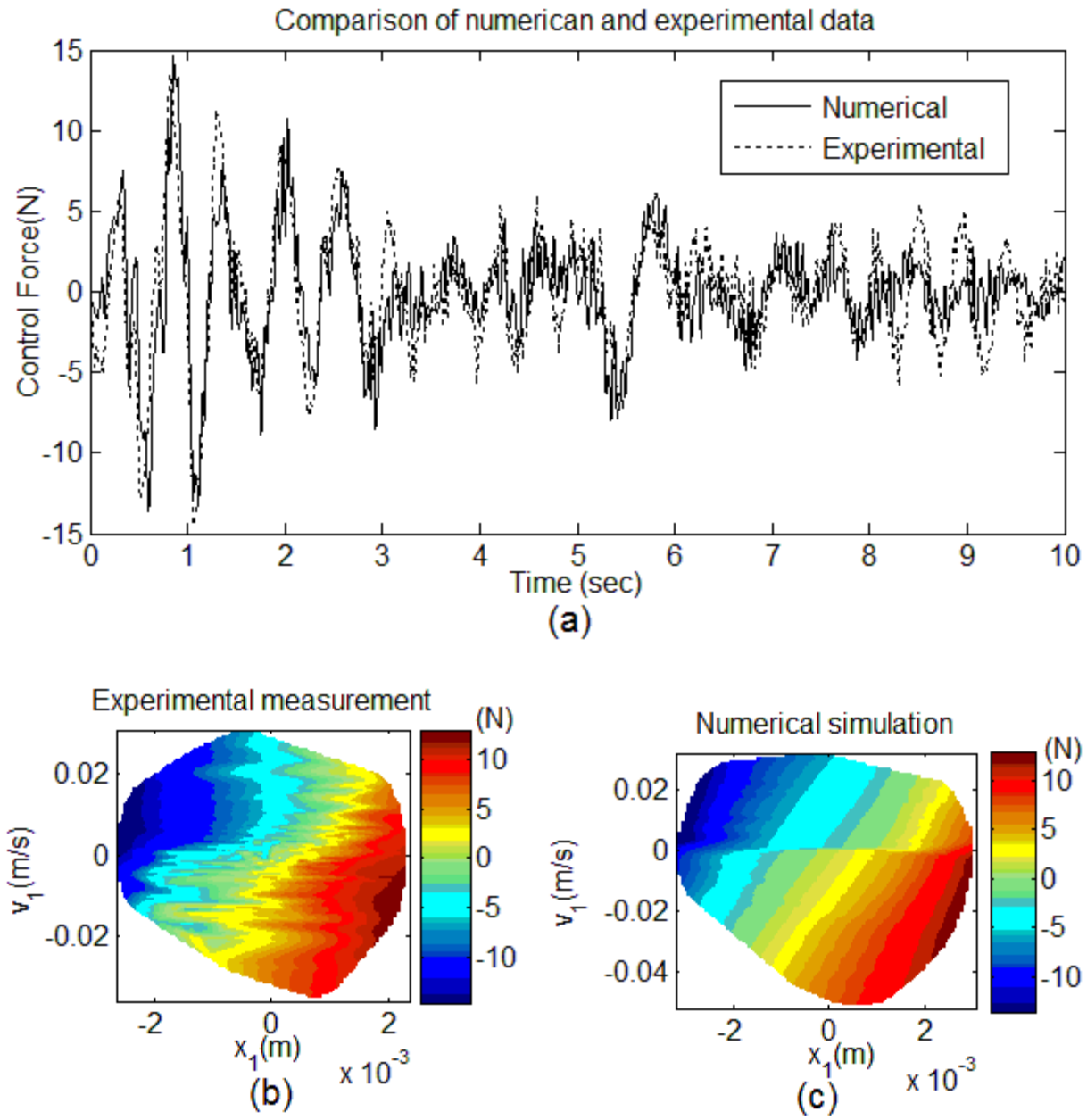

Figure 11. Comparison of the model simulation and the experimental measurement with the 1940 El Centro earthquake applied on the three-story structure equipped with bio-inspired passive actuator: (a) Comparison of the control force output over time; (b) FDV plot of the experimental measurement; (c) FDV plot of the numerical simulation.

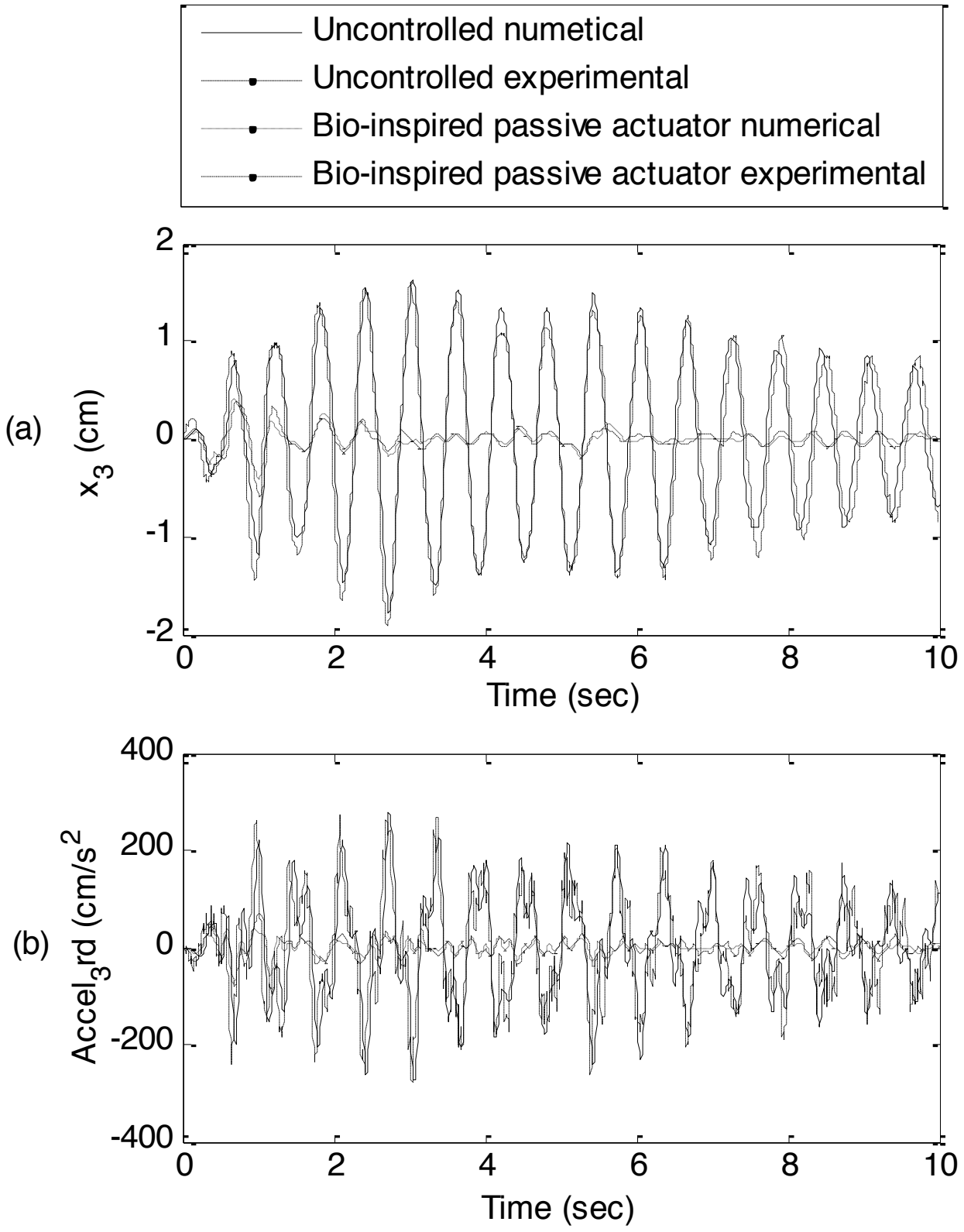

Figure 12. Comparison of numerical prediction and experimental measurement of the third floor responses in (a) displacement and (b) acceleration of both uncontrolled and controlled with the bio-inspired passive actuated systems due to the El Centro earthquake as shown in figure 2.

6. Assessing performance of mechanical negative spring with other state-of-the-art actuators

The experimental validation of the numerical model of the current new bio-inspired passive actuator, can now be used for more evaluations of the actuator's structural response reduction performance on more structures. A structural model of a scaled, three-story, test structure as described in Dyke *et al* 1995 and Dyke *et al* 1996a, is used for the assessment, and the peak responses of displacements, drifts, and accelerations are compared with the results of other state-of-the-art actuators. In this simulation, the model structure is subjected to the north-south component of the 1940 El Centro earthquake. Because the system is a scaled model, the earthquake is scaled in time to five times the recorded rate. The parameters of the new bio-inspired passive actuator, configured to fit the new structure, are displayed in table 2.

Table 2. Parameters of the bio-inspired passive actuator, tailored for the model structure described in Dyke *et al* 1995 and Dyke *et al* 1996a.

Parameter	Value	Parameter	Value
r	0.004763 m	θ	45˚
PL	1500 N	C_0	15000 N s/m

The maximum structural responses to the El Centro earthquake are presented in table 3. Here, x_i is the displacement of the ith floor relative to the ground, d_i is the interstory drift (i.e., $x_i - x_{i-1}$), $\ddot{x}_{ai}$ is the absolute acceleration of the ith floor, and f is the applied control force. It is noticed that the new bio-inspired passive actuator employing the mechanical negative spring has a comparable performance of reducing displacements and drifts as compared to other state-of-the-art actuators including the former bio-inspired passive actuator. Certainly, the fundamental concept of using bio-inspired abalone shell mechanism to design passive controllers is worth further research and development.

Since the comparisons of the results by various methods are made only for this one specific example or model, they may be by no means generally and definitely conclusive. However, these comparisons do provide an evidence of data that the current bio-inspired passive actuator can deliver performance and effectiveness that are comparable to the state-of-the-art active and semi-active actuators.

Table 3. Comparisons of peak responses of displacements, drifts, and accelerations over the time-scaled 1940 El Centro earthquake using (a) active LQR control; (b) new bio-inspired passive actuator employing mechanical negative spring; (c) former bio-inspired passive actuator using magnetic negative spring (Yang *et al* 2010); (d) semi-active magnetorheological (MR) damper (Dyke *et al* 1996b); (e) semi-active brushless DC machine (Scruggs and Iwan 2003).

		No control	Active LQR optimal control	Current Bio-inspired passive actuator	Previous Bio-inspired Passive actuator	Semi-active MR damper	Semi-active BDC
			(a)	(b)	(c)	(d)	(e)
Displacement (cm)	x_1	0.549	0.093	0.111	0.108	0.114	0.103
	x_2	0.837	0.139	0.146	0.149	0.185	0.152
	x_3	0.973	0.191	0.219	0.202	0.212	0.198
Drift (cm)	d_1	0.549	0.093	0.111	0.108	0.114	0.103
	d_2	0.318	0.093	0.106	0.090	0.090	0.088
	d_3	0.203	0.065	0.076	0.068	0.101	0.060

Acceleration (cm/s^2)	$\ddot{x}_{d1}$	1039	450	288	319	696	250
	$\ddot{x}_{d2}$	1096	500	301	520	739	253
	$\ddot{x}_{d3}$	1480	637	533	629	703	417
Max force (N)	f	0	941	767	763	941	749

7. Design case study for full scale structure

To assess the feasibility of a scaled magnetic and that of mechanical negative spring actuator, a design case study was conducted for a scaled application. A sample control system design simulation is performed to check the feasibility of permanent magnet as a primary material for negative spring force. For this simulation, a single bay, three-story structure in the text by Biggs (1964) is used. The structure is 10.668 m tall, and weighs a total of 5.93×10^4 kg. More detailed structure properties are discussed and analyzed in Wrobleski *et al*. (2003) A bio-inspired passive actuator is designed to reduce the first floor displacement and the third floor acceleration. The actuator requires a negative spring with capacity of 30 kN. A negative spring actuator using magnets with such capacity would require roughly 870 kg of Neodymium magnets. Parameters used for this calculation are listed in table 4. High strength permanent magnets, such as neodymium magnets, are categorized as rare earth material which has limited flexibility for increasing global supply (U.S. Department of Energy 2011), leading to a higher cost than conventional springs.

Table 4. Parameters of the magnetic negative spring actuator used for assessing feasibility.

Parameter	Value
B_0	1 Tesla
μ_0	$4\pi\times10^{-7}$ T·m/A
R	10 cm
L	10 cm
l_1	-3 cm
l_2	3 cm
Density	7.4 g/cm^3
Total mass	870 kg

Using conventional spring, it becomes affordable to build a negative spring actuator with the same capacity. A mechanical negative spring with 30kN capacity would require a steel triangular ramp with 45 degree ramp angle, and a conventional spring with maximum capacity of 30kN or more. This requirement is easily achieved with off-the-shelf springs, for example, using three 10kN capacity springs from SODEMANN Industrial springs Corp. (ST53610) in parallel. Custom designing for springs with higher strength is also possible with spring rate formula

$$k_{spring} = \frac{GD_{wire}^4}{8\left(D_{outer} - D_{wire}\right)^3 n_{coil}} \tag{13}$$

where k_{spring} is the spring constant, G is the shear modulus, D_{outer} is the outer diameter of spring, D_{wire} is the diameter of spring wire, and n_{coil} is the number of active coils.

8. Conclusion

The structural response reduction performance evaluation and experimental verification of the mathematical model of the bio-inspired passive control system has been studied. A new bio-inspired passive actuator was designed using the linear quadratic regulator optimization and the force-displacement-velocity plots, as proposed in Yang *et al*. 2010. The current mathematical model of the new design is able to predict the behavior and the system response using a specifically chosen N-S component of El Centro earthquake excitation.

The bio-inspired passive actuator has demonstrated an excellent performance on reducing the structural response. Mimicking the FDV profile of an optimal control and implementing the mechanism of negative sacrificial bond-hidden length suggests a new paradigm of designing actuators, and its effectiveness has been studied and compared with the state-of-the-art research results. The bio-inspired passive actuator has demonstrated performance that is noteworthy considering that the passive actuator uses no external power, and that a power outage could occur during earthquake. The proposed bio-inspired actuator using mechanical negative spring has shown improvements over the former bio-inspired passive actuator using magnetic negative spring in reducing peak acceleration. Although passive, the bio-inspired actuators are comparable in performance to state-of-the-art semi-active actuators in numerical simulations.

The significance of the current design of negative spring actuator is the usage of conventional spring for generating negative spring force output. As compared to permanent magnets, a conventional spring is readily available, it can be scaled to output very high forces, and is much cheaper than magnets that can have the same magnitude of force. This allows the bio-inspired passive actuator produce output force up to hundreds of thousands of pounds using parallel connection of industrial springs. Such high capacity of force makes the bio-inspired passive actuator implementable for a wide spectrum of applications ranging from building small proof-of-concept dynamic systems to vehicle suspension, civil structures including highway bridges and buildings, and even aeronautical vehicles, in a practical manner.

Acknowledgements

This study is sponsored by the National Science Foundation grant CMMI-1014958. The guidance of program director, Dr. B. M. Kramer, is gratefully acknowledged. The authors acknowledge Daniel Bridge, research assistant, for his help in setting up shake table and data acquisition.

REFERENCES

Becker, N., Oroudjev, E., Mutz, S., Cleveland, J. P., Hansma, P. K., Hayashi, C. Y., Makarov, D. E., and Hansma, H. G. (2003). "Molecular nanosprings in spider capture-silk threads." *Nature Materials*, **2(4)**, 278-283.

Biggs, J. M. (1964). *Introduction to structural dynamics*, (New York:McGraw-Hill)

Chen, C., and Chen, G. (2004). "Shake table tests of a quarter-scale three-storey building model with piezoelectric friction dampers." *Structural Control and Health Monitoring*, **11(4)**, 239-257.

Craig R R Jr 1981 *Structural Dynamics* (New York:Wiley)

Dyke, S. J., Caicedo, J. M., Turan, G., Bergman, L. A., Hague, S. (2003). "Phase I Benchmark Control Problem for Seismic Response of Cable-Stayed Bridges." *J. Struct. Eng.*, **129(7)**, 857–872.

Dyke, S. J., Spencer, B. F., Quast, P., and Sain, M. K. (1995). "The role of control–structure interaction in protective system design." *J. Eng. Mech. ASCE* **121** 322–38

Dyke, S. J., Spencer, B. F., Quast, P., Kaspari, D. C. and Sain, M. K. (1996a). "Implementation of an active mass driver using acceleration feedback control Microcomputers in Civil Engineering." *(Special issue on Active and Hybrid Structural Control)* **11** 305–23

Dyke, S. J., Spencer, B. F., Sain, M. K., and Carlson, J. D. (1996b). "Modeling and control of magnetorheological dampers for seismic response reduction." *Smart Materials and Structures*, **5**, 565-575.

Dyke, S. J., Spencer, B. F., Sain, M. K., and Carlson, J. D. (1998). "An experimental study of MR dampers for seismic protection." *Smart Materials and Structures*, **7**, 693-703.

Evans, A. G., Suo, Z., Wang, R. Z., Aksay, I. A., He, M. Y., and Hutchinson, J. W. (2001). "Model for the robust mechanical behavior of nacre." *Journal of Materials Research*, **16(9)**, 2475-2484.

Fantner, G. E., Adams, J., Turner, P., Thurner, P. J., Fisher, L. W., and Hansma, P. K. (2007). "Nanoscale ion mediated networks in bone: Osteopontin can repeatedly dissipate large amounts of energy." *Nano Letters*, **7(8)**, 2491-2498.

Fantner, G. E., Hassenkam, T., Kindt, J. H., Weaver, J. C., Birkedal, H., Pechenik, L., Cutroni, J. A., Cidade, G. A. G., Stucky, G. D., Morse, D. E., and Hansma, P. K. (2005). "Sacrificial bonds and hidden length dissipate energy as mineralized fibrils separate during bone fracture." *Nature Materials*, **4(8)**, 612-616.

Fantner, G. E., Oroudjev, E., Schitter, G., Golde, L. S., Thurner, P., Finch, M. M., Turner, P., Gutsmann, T., Morse, D. E., Hansma, H., and Hansma, P. K. (2006a). "Sacrificial bonds and hidden length: Unraveling molecular mesostructures in tough materials." *Biophysical Journal*, **90(4)**, 1411-1418.

Fantner, G. E., Rabinovych, O., Schitter, G., Thurner, P., Kindt, J. H., Finch, M. M., Weaver, J. C., Golde, L. S., Morse, D. E., Lipman, E. A., Rangelow, I. W., and Hansma, P. K. (2006b). "Hierarchical interconnections in the nano-composite material bone: Fibrillar cross-links resist fracture on several length scales." *Composites Science and Technology*, **66(9)**, 1205-1211.

Fritz, M., Belcher, A. M., Radmacher, M., Walters, D. A., Hansma, P. K., Stucky, G. D., Morse, D. E., and Mann, S. (1994). "Flat Pearls from Biofabrication of Organized Composites on Inorganic Substrates." *Nature*, **371(6492)**, 49-51.

Gebeshuber, I. C., Kindt, J. H., Thompson, J. B., Del Amo, Y., Stachelberger, H., Brzezinski, M. A., Stucky, G. D., Morse, D. E., and Hansma, P. K. (2003). "Atomic force microscopy study of living diatoms in ambient conditions." *Journal of Microscopy-Oxford*, **212**, 292-299.

General Electric 2010 *Response to Department of Energy Request for Information* (Fairfield, CT)
Gilbert, W 1600 *On the Magnet and Magnetic Bodies, and on That Great Magnet the Earth*
Gutsmann, T., Hassenkam, T., Cutroni, J. A., and Hansma, P. K. (2005). "Sacrificial bonds in polymer brushes from rat tail tendon functioning as nanoscale velcro." *Biophysical Journal*, **89(1)**, 536-542.
Hansma, P. K., Fantner, G. E., Kindt, J. H., Thurner, P. J., Schitter, G., Turner, P. J., Udwin, S. F., and Finch, M. M. (2005). "Sacrificial bonds in the interfibrillar matrix of bone." *J Musculoskelet Neuronal Interact*, **5(4)**, 313-315.
Hansma, P. K., Turner, P. J., and Ruoff, R. S. (2007). "Optimized adhesives for strong, lightweight, damage-resistant, nanocomposite materials: new insights from natural materials." *Nanotechnology*, **18(4)**.
Hassenkam, T., Gutsmann, T., Hansma, P., Sagert, J., and Waite, J. H. (2004). "Giant bent-core mesogens in the thread forming process of marine mussels." *Biomacromolecules*, **5(4)**, 1351-1355.
Housner, G. W., Bergman, L. A., Caughey, T. K., Chassiakos, A. G., Claus, R. O., Masri, S. F., Skelton, R. E., Soong, T. T., Spencer, B. F., and Yao, J. T. P. (1997). "Structural Control: Past, Present, and Future." *Journal of Engineering Mechanics, ASCE*, **123(9)**, 897-971.
Jackson, A. P., Vincent, J. F. V., and Turner, R. M. (1988). "The Mechanical Design of Nacre." *Proceedings of the Royal Society of London Series B-Biological Sciences*, **234(1277)**, 415-&.
Kwakernaak, H., and Sivan, R. (1972). *Linear optimal control systems*, (New York:Wiley-Interscience)
LabVIEW 8 National Instruments Corporation, (Austin, TX)
MATLAB R2011b The Math Works, Inc., (Natick, MA)
Schaffer, T. E., IonescuZanetti, C., Proksch, R., Fritz, M., Walters, D. A., Almqvist, N., Zaremba, C. M., Belcher, A. M., Smith, B. L., Stucky, G. D., Morse, D. E., and Hansma, P. K. (1997). "Does abalone nacre form by heteroepitaxial nucleation or by growth through mineral bridges?" *Chemistry of Materials*, **9(8)**, 1731-1740.
Scruggs, J. T., and Iwan, W. D. (2003). "Control of a Civil Structure Using an Electric Machine with Semiactive Capability." *Journal of Structural Engineering*, **129(7)**, 951-959.
Shigley, J. E., Budynas, R. G., Mischke, C. R. (2003) *Mechanical Engineering Design 7th edition* (Springfield, IL:McGraw-Hill)
Smith, B. L., Schaffer, T. E., Viani, M., Thompson, J. B., Frederick, N. A., Kindt, J., Belcher, A., Stucky, G. D., Morse, D. E., and Hansma, P. K. (1999). "Molecular mechanistic origin of the toughness of natural adhesives, fibres and composites." *Nature*, **399(6738)**, 761-763.
Soong, T. T., and Costantinou, M. C. (1994). *Passive and Active Structural Vibration Control in Civil Engineering*, (New York:Springer-Verlag)
Soong, T. T., and Spencer, B. F. (2002). "Supplemental energy dissipation: state-of-the-art and state-of-the-practice." *Engineering Structures*, **24**, 243-259.
Spencer, B. F., Dyke, S. J., Sain, M. K., and Carlson, J. D. (1997). "Phenomenological Model for Magnetorheological Dampers." *Journal of Engineering Mechanics*, **123(3)**, 230-238.
Spencer, B. F., Jr., Dyke, S. J., and Deoskar, H. S. (1998). "Benchmark Problems in Structural Control: Part 1-Active Mass Driver System." *Earthquake Engrn. Struct. Dyn.*, **27(11)**, 1127-1139.
Spencer, B. F., Jr., and Nagarajaiah, S. (2003). "State of the Art of Structural Control." *J. Struct. Engrg.*, **129(7)**, 845-856.
Sun, C., Fantner, G. E., Adams, J., Hansma, P. K., and Waite, J. H. (2007). "The Role of Calcium and Magnesium in the Concrete Tubes of the Sandcastle Worm." *J. Experimental Biology,* **210(8)**, 1481-1488
Thompson, J. B., Kindt, J. H., Drake, B., Hansma, H. G., Morse, D. E., and Hansma, P. K. (2001). "Bone indentation recovery time correlates with bond reforming time." *Nature*, **414(6865)**, 773-776.
Thurner, P. J., Erickson, B., Jungmann, R., Schriock, Z., Weaver, J. C., Fantner, G. E., Schitter, G., Morse, D. E., and Hansma, P. K. (2007). "High-speed photography of compressed human trabecular bone correlates whitening to microscopic damage." *Engineering Fracture Mechanics*, **74(12)**, 1928-1941.
Thurner, P. J., Erickson, B., Schriock, Z., Langan, J., Scott, J., Zhao, M., Weaver, J. C., Fantner, G. E., Turner, P., Kindt, J. H., Schitter, G., Morse, D. E., and Hansma, P. K. (2006). "High-speed

photography of the development of microdamage in trabecular bone during compression." *Journal of Materials Research*, **21(5)**, 1093-1100.

U.S. Department of Energy *2011 Critical Materials Strategy*

Wrobleski, M. S., Yang, H. T. (2003). "Identification of Simplified Models Using Adaptive Control Techniques." *J. Struct. Engrg.*, **129(7)**, 989–997.

Yang, H. T., Lin, C., Bridges, D., Randall, C. J., Hansma, P. K (2010). "Bio-inspired passive actuator simulating an abalone shel mechanism for structural control." *Smart Materials and Structures*, **19**, 105011.

Zaremba, C. M., Belcher, A. M., Fritz, M., Li, Y. L., Mann, S., Hansma, P. K., Morse, D. E., Speck, J. S., and Stucky, G. D. (1996). "Critical transitions in the biofabrication of abalone shells and flat pearls." *Chemistry of Materials*, **8(3)**, 679-690.